https://doi.org/10.15407/ujpe71.8.682

O.YA. OLIKH

Taras Shevchenko National University of Kyiv
(64/13, Volodymyrska Str., Kyiv 01601, Ukraine; e-mail: olegolikh@knu.ua)

MACHINE LEARNING MODELS FOR EVALUATING EFFICIENT CARRIER MOBILITY IN SILICON

The application of machine learning (ML) models – specifically Random Forest (RF), Gradient Boosting (GB), Support Vector Regression (SVR), and Deep Neural Networks (DNNs) – alongside Symbolic Regression (SR) for predicting carrier mobility in monocrystalline silicon over wide temperature (200–500 K) and doping concentration (10^{13}–10^{19} cm^{-3}) ranges has been evaluated. The analytical expressions derived via SR are notably more parsimonious, requiring 50% fewer parameters than the Klaassen model. Furthermore, these expressions bypass the need for preliminary impurity ionization calculations while maintaining a relative error below 0.1% in most cases. A comparative analysis demonstrated that the SR and SVR models significantly outperform the Arora approximation in terms of accuracy, particularly for minority carriers. The proposed approach offers a robust framework for TCAD systems, substantially reducing computational overhead while ensuring high modeling accuracy.

K e y w o r d s: carrier mobility, silicon, Klaassen model, symbolic regression, machine learning.

1. Introduction

The mobility μ of charge carriers is one of the key transport parameters of semiconductors, which directly determines the efficiency of electric charge transfer under the action of an external electric field. Quantitatively, the mobility μ relates the drift velocity of carriers to the field strength and, at a fixed carrier concentration, just this value governs the level of conductivity in the material and the suitability of the latter for application in active electronic elements. In a physical sense, mobility is a bridge between microscopic mechanisms of carrier scattering and macroscopic electrophysical characteristics. From an applied point of view, mobility determines the velocity and energy efficiency of electronic components, affects the carrier diffusion length, being therefore a critical parameter for field-effect transistors, solar cells, LEDs, *etc.* In particular, an analysis of the mechanisms that limit the mobility makes it possible to identify the dominant scattering channels and optimize the technological parameters of material growth and treatment.

In addition, mobility is a fundamental parameter when modeling transport processes in semiconductor structures, and the ability to evaluate it depending on the temperature, impurity concentration, and electric field is necessary for adequate prediction of device characteristics, including degradation effects. Mobility has to be known (can be evaluated) when interpreting experimental data. It is necessary to resolve the influence of concentration and scattering, to process the measurement results of the Hall effect, magnetoresistance, and frequency dependence

C i t a t i o n: Olikh O.Ya. Machine learning models for evaluating efficient carrier mobility in silicon. *Ukr. J. Phys.* **71**, No. 8, 682 (2026). https://doi.org/10.15407/ujpe71.8.682.

of capacitance or conductivity, and to establish the dominant scattering mechanism, which is extremely important when developing new materials, nanostructures, and radiation-resistant systems.

The most general approach to calculating the value of μ is based on solving the Boltzmann kinetic equation, taking into account the real band structure of the semiconductor. This way involves, in particular, the calculation of a collision integral, which makes allowance for all available mechanisms of carrier scattering (by phonons of various types, ionized and neutral impurities, dislocations, grain boundaries, other carriers, surfaces, *etc.*). It is clear that such an approach is quite complicated, being far from always justified in terms of the effort involved, which necessitates the application of various approximations. In particular, in the framework of the relaxation time approximation, the exponential relaxation to equilibrium is assumed, which allows the collision integral to be replaced by a simple expression using the characteristic time. In so doing, if an isotropic semiconductor with parabolic zones is considered, and the relaxation time is assumed to be independent on energy, then [1]

$$\mu = \frac{e\tau_p}{m_\sigma}, \tag{1}$$

where e is the elementary charge, τ_p the carrier momentum relaxation time, and m_σ the effective mass of electrical conductivity. In the case where different scattering processes are statistically independent, the Matthiessen's rule can be applied [2],

$$\mu^{-1} = \sum_i \mu_i^{-1}, \tag{2}$$

where μ_i is the carrier mobility if only the i-th scattering mechanism is active.

For the vast majority of scattering mechanisms, expressions for evaluating the carrier mobility are known. For example, the Brooks–Herring or Conwell–Weisskopf formulas [1, 3, 4] are often used to describe scattering by ionized impurities. In the case of carrier-carrier scattering, the approach developed by Fletcher [5, 6] is applied; see Appendix A. However, in most cases, the approach to evaluating the carrier mobility, which is based on the application of the Matthiessen's rule and a set of "single-mechanism" formulas, is not practically applicable, since for an accurate description of a real material, a substantial number of mechanisms have to be taken into account, which, moreover, are modified depending on which carrier (the electron or the hole) is considered, and what role (major or minor) it plays. As a result, an approach to evaluating the value of μ that involves the use of an approximation function has become more widespread. Such a function is usually constructed on the basis of experimental data, and its analytical form and the set of parameters are determined by the properties of a particular material.

For single-crystalline silicon (the case of weak fields and a bulk semiconductor, without taking surface effects into account), one of the first such approximations was the expression proposed by Caughey and Thomas [7,8]. It was assumed that the differences between the electron and hole mobilities are taken into account through different values of the corresponding parameters within the same analytical dependence; see Appendix B. The Caughey–Thomas formula was primarily proposed to evaluate the dependence of the majority carrier mobility on the dopant concentration near a temperature of 300 K, but it does not allow one to evaluate the mobility of minority carriers and does not take into account the temperature dependence of μ; therefore, it has limited applicability. The modified Masetti version provides the application of various expressions to describe the electron and hole mobilities (see formulas (B2) below), as well as the dependence on specific doping atoms [9, 10]. Masetti's theory describes the experimental data better than the Caughey–Thomas approach does, but it also does not allow obtaining information for minority carriers and temperatures other than room temperature. An attempt to take temperature dependences into account was made by N. Arora and co-authors [11]. In the cited work, scattering by phonons and ionized impurities was analyzed, and the generalized Caughey–Thomas expression was used to describe the concentration dependence of mobility, the analytical form of which is identical for electrons and holes; see formulas (B3)–(B4) below.

However, the best agreement with experimental data is provided by the approach to mobility evaluation developed by Klaassen [12] (it also known in the literature as the Philips Unified model) and implemented in the modern Sentaurus and Silvaco packages. Within this approach, scattering by lattice vibrations, ionized impurities, and other charge carriers

is considered to be the determining mechanism. The mobility is calculated using relationships formulated separately for electrons and holes, as well as for majority and minority carriers. The formulas are multicomponent (structurally branched) and contain more than twenty parameters; see Appendix C. This fact, of course, does not create insurmountable difficulties but leads to a situation when the simpler Arora approach (formulas (B3)–(B4)) is often used in practice, despite its lower accuracy, to evaluate the mobility of charge carriers in silicon. Note that in the original work [11], the expressions were obtained, and the values of the constants were determined based on the analysis of experimental data for the mobility of majority carriers at various temperatures and doping levels. Often the formulas are applied to minority carriers, using the values of the constants obtained in works [13] (for electrons) and [14] (for holes); see Table B3. However, in the cited works, the data are given only for one temperature; therefore, the extension of the expressions to a wide temperature interval is somewhat presumptuous.

Note that the issue of describing the carrier mobility continues to attract attention, and new models appear periodically. Some of them specify approaches to describe scattering according to a specific mechanism [15], or in structures with a limited dimension [16, 17]; others offer universal expressions that allow the incorporation of additional scattering mechanisms through modifying existing models [18–20], use approximation polynomials [21], or are based on first principles [2, 22].

As with most aspects of semiconductor physics [23], the task of studying the charge carrier mobility has recently often been solved using machine learning (ML) methods, among which several key domains can be distinguished. First, the application of computationally efficient surrogate models makes it possible to substantially simplify resource-intensive calculations of transport processes from first principles or the solution of the Boltzmann equation; in particular, deep [24] and physically informed neural networks [25, 26] are used, and in the latter case, the structure of differential equations is directly integrated into the learning process. Second, the exact determination of mobility is no less difficult a task than its modeling, and in this regard, a number of ML approaches have been proposed to analyze the results of measurements [27] and improve their implementation procedures [28]. Third, the knowledge transfer approach makes it possible to leverage a large dataset of well-studied bulk materials (e.g., silicon) to predict the properties of new systems, in particular, two-dimensional crystals [29], for which the calculation of mobility from first principles is extremely difficult. Finally, ML models are being developed to predict mobility based on a set of physical descriptors (lattice symmetry, bulk geometry of molecules, number of valence electrons, electron-phonon coupling constant, band gap, etc.) [30–35]. The latter option corresponds to a common approach to modeling and optimizing various semiconductor materials and devices [36–38].

The aim of this work is to create regression ML models capable of evaluating the charge carrier mobility in single-crystalline silicon and its dependence on the temperature T and the dopant concentration N_D. Such models combine the simplicity of calculations, which is characteristic of the Arora approach, with a high accuracy of predictions, which is the main advantage of the Klaassen model. The proposed approach can be adapted to a specific set of experimental data or to the results of fundamental calculations, for example, in the framework of solving the Boltzmann equation.

Furthermore, the application of the symbolic regression algorithm made it possible to obtain considerably simpler analytical expressions for describing the mobility than those in the Philips model, providing the physically correct behavior of the dependencies in a wide range of temperatures and concentrations. Such an approach has a number of advantages. First, the formation of a single unified description of carrier mobility without the need for explicit combination of individual scattering mechanisms through the Matthiessen's rule simplifies the algorithmic implementation in packages such as TCAD and reduces the risk of accumulating errors when switching between various doping regimes or temperatures. Second, the compact analytical form substantially reduces computational costs in multidimensional numerical simulations, where the mobility is calculated at every grid node at every step of the iterative process. Third, the obtained expressions for the mobility depend on only two parameters (T and N_D) and are analytically differentiable, which makes it possible to ensure the stability and convergence of iterative algorithms at the stage of the numerical solution of the transport equations, obtain correct deriva-

tives of transport coefficients, facilitate the derivation of simplified physical models for rapid engineering analysis, diminish the errors associated with numerical differentiation, and increase the efficiency of gradient methods in the problems of parametric optimization of technological parameters. Therefore, the use of regression-based machine learning allows for a compromise between the physical interpretability, numerical efficiency, and high accuracy of the description of the silicon transport properties, which makes the proposed approach promising for both fundamental research and applied device modeling.

2. Methodology

2.1. Features of data preparation

To build ML models, a representative dataset is required first of all. In this work, such data were the mobility values corresponding to the specified temperatures and dopant concentrations. Both the training and test sets were formed by calculating the mobility according to formulas (C1)–(C10). That is, the results obtained in the framework of the Klaassen model were taken as reference, and the regression models were trained so that their predictions closely reproduced those values.

The models capable of predicting the mobility of both majority and minority electrons and holes in silicon were developed. Separate training and test data sets were formed in each of those four cases. In what follows, the mobility of electrons in n-Si is denoted as μ_{nn}, and as μ_{np} in p-Si. Similarly, the quantities μ_{pp} and μ_{pn} correspond to the mobilities of holes as majority and minority charge carriers, respectively.

When calculating the mobility value, the crystal was assumed to contain only one type of dopant impurities, i.e., an uncompensated semiconductor was considered, and the presence of non-equilibrium charge carriers was neglected. As can be seen from expressions (C1)–(C10), the mobility depends on the electron, n, and hole, p, concentrations, as well as on the number of ionized acceptors, N_a^-, and donors, N_d^+, per unit volume. In the case of n-Si, the following expressions were used to calculate the charge carrier concentrations:

$$n = \frac{N_d^+}{2} + \sqrt{\left(\frac{N_d^+}{2}\right)^2 + n_i^2}, \quad p = \frac{n_i^2}{n}, \tag{3}$$

and the temperature dependence of the electron concentration in the intrinsic semiconductor, n_i, was calculated according to Ref. [39]. In turn, the concentration of ionized donors was calculated taking into account the Fermi–Dirac statistics,

$$N_d^+ = N_d \left(1 - \frac{1}{1 + 0.5 \exp\left[\frac{E_\mathrm{F} - E_d}{kT}\right]}\right), \tag{4}$$

where E_F is the Fermi level position, and E_d the donor level energy. The Fermi level location was evaluated using the electroneutrality condition

$$n = p + N_d^+. \tag{5}$$

In doing so, it was assumed that

$$n = N_C F_{\frac{1}{2}}\left(-\frac{E_\mathrm{F}}{kT}\right), \quad p = N_V F_{\frac{1}{2}}\left(-\frac{E_G - E_\mathrm{F}}{kT}\right), \tag{6}$$

where N_C and N_V are the effective densities of states near the conduction band bottom and the valence band top, respectively (they were calculated according to Ref. [39]), E_G the band gap width (it was calculated according to [40]), and $F_{\frac{1}{2}}$ the Fermi–Dirac integral of degree $1/2$ (it was evaluated using the approximation from Ref. [41]).

In the case of p-Si, the calculations were performed similarly. For both electron and hole semiconductors, the dopant activation energy was assumed to be 45 meV. This value corresponds to the ionization energies of boron and phosphorus atoms, which are the main dopants for silicon.

Note that the following temperature intervals and doping levels were considered in the work:

$$T = (200 \div 500)\ \mathrm{K}, \quad N_D = \left(10^{13} \div 10^{19}\right)\ \mathrm{cm}^{-3}, \tag{7}$$

which correspond to the Klaassen theory applicability region. Note that the indicated approach to calculate the concentrations of charged components in the crystal allowed deviations from the approximate relationships $n = N_d^+ = N_d$ (for n-Si) and $p = N_a^- = N_a$ (for p-Si) to be taken into account, which, in general, can be used only within the interval from the impurity depletion temperature to the onset temperature of intrinsic conductivity. As the estimates show, for boron and phosphorus, the depletion temperature is higher than 200 K at $N_D \geq 10^{18}$ cm^{-3}, and at $N_D < 3 \times 10^{14}$ cm^{-3}, the temperature at which intrinsic charge carriers cannot be neglected is lower

than 500 K. Therefore, the application of the strict approach (3)–(6) is necessary.

When creating each of the four training datasets, 500 pairs of (T, N_D)-values were randomly selected from the interval (7), and the μ-values were calculated using expressions (C1)–(C10) and (3)–(6). The test sets used to evaluate the quality of model predictions included 2550 samples each; they corresponded to all combinations of 51 temperature values from 200 K to 500 K with a step of 6 K, and 50 doping levels uniformly distributed on a logarithmic scale from 10^{13} cm^{-3} to 10^{19} cm^{-3}.

2.2. Applied machine learning models

To find analytical expressions for the mobility, the Symbolic Regression (SR) algorithm was used [42]. This is a relatively new ML algorithm that allows approximating the relationships between input and output parameters without prior specification of the analytical form of the approximating function. The formation of the functional dependence and the selection of its numerical parameters were carried out using evolutionary metaheuristic algorithms [43]. SR is a method that combines experimental data, ML models, and scientific theories, and provides interpretable analytical expressions that require less computational effort as compared to classical ML models and can be more easily integrated into the solution of a wide scope of physical problems [43–48].

The algorithm was implemented in Python using the PySR package [49]. Standard mathematical functions ($+$, $-$, $\times$, $\div$, exp, ln, x^y, tanh, sin) and real constants were used to construct the equations. In addition, specially constructed operators $f_1(x) = \frac{1}{1+x}$ and $f_2(x,y) = \frac{x \cdot y}{x+y}$ were used, which correspond to functions that are often found in existing models for describing the mobility of charge carriers; see Appendices. The preprocessing of data involved their normalization: as the SR model input, the dimensionless quantities

$$T_n = \frac{T}{300\,\mathrm{K}} \text{ and } N_{Dn} = \frac{N_D}{10^{17}\,\mathrm{cm}^{-3}} \tag{8}$$

were used.

In addition, several regression models were developed that use various ML algorithms, in particular, Random Forest (RF), Gradient Boosting (GB), Support Vector Regression (SVR), and Deep Neural Network (DNN). For each indicated algorithm, two model variants were prepared, which differed in the data preprocessing. In one case, the normalized values of temperature and dopant concentration were used as input parameters (see formulas (8)), and the predictions were oriented toward obtaining the μ-value. The corresponding models will be designated below by adding the suffix _N to the abbreviation of the applied algorithm (RF_N, DNN_N, and so forth). For the second type of models, it was taken into account that an obstacle to accurate predictions may be a wide range of used features (for example, N_D varies within six orders of magnitude). Therefore, in this case, the preprocessing of input data involved the normalization of the temperature values T and the logarithms of the doping degree $\lg N_D$; the quantity $\lg \mu$ was considered as the target variable. As a result, the training sets of each input and output feature were characterized by the zero mean deviation and the standard deviation of unity. The notations for the corresponding models will contain the suffix _S (RF_S, DNN_S, and so forth).

The models were implemented in Python using the Keras and Scikit-learn packages. To adjust the hyperparameters of the models, which is known to be extremely important for optimizing their performance [50], the Optuna package [51] was applied together with the TPE sampler, Hyperband pruner, and fivefold cross-validation.

It should be emphasized that although the above regression approach is widely used in various fields of physics, such models are actually "black boxes", which substantially complicates the justification of the obtained results. Therefore, such models are gradually becoming less satisfactory to researchers.

2.3. Evaluation metrics

To assess the predictive properties of the models, several metrics were used, namely, the mean squared error (MSE), the mean absolute error (MAE), and the mean absolute percentage error (MAPE). They are defined by the following expressions:

$$\mathrm{MSE} = \frac{1}{N}\sum_{i=1}^{N}(\hat{y}_i - y_i)^2, \tag{9}$$

$$\mathrm{MAE} = \frac{1}{N}\sum_{i=1}^{N}|\hat{y}_i - y_i|, \tag{10}$$

$$\mathrm{MAPE} = \frac{1}{N}\sum_{i=1}^{N}\frac{|\mu_i^{\mathrm{PRED}} - \mu_i^{\mathrm{TRUE}}|}{\mu_i^{\mathrm{TRUE}}} \times 100\%, \tag{11}$$

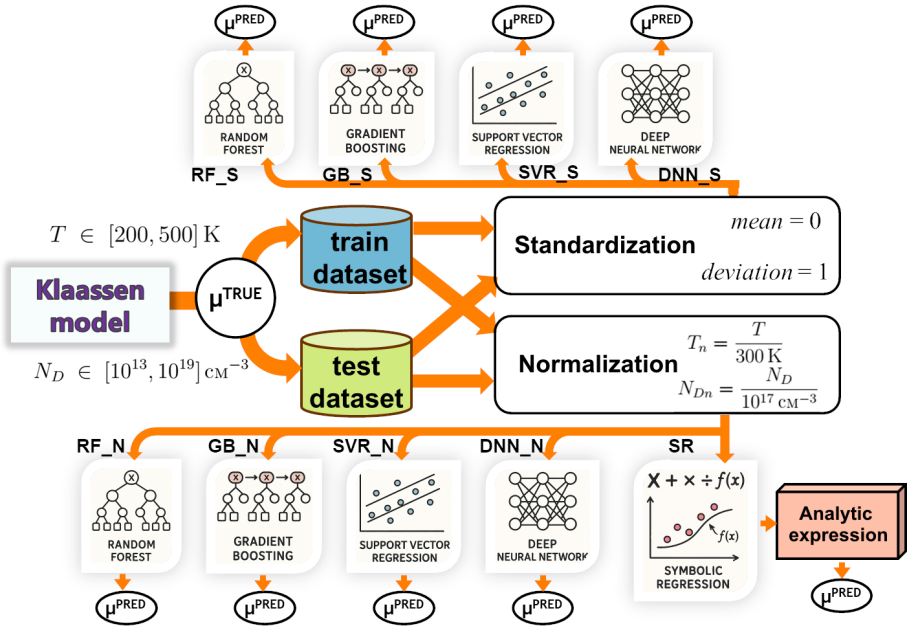

Fig. 1. General schematic diagram of calculations

where $\hat{y}_i$ is the model-predicted value for the i-th sample (the set of input parameters), y_i the known target value for the i-th sample (for the SR and $*_{\mathrm{N}}$ models, it coincided with the mobility value; for the $*_{\mathrm{S}}$ models, it appeared as a result of logarithmization and standardization), N the number of samples in the dataset, μ_i^{PRED} the predicted mobility value (for the $*_{\mathrm{S}}$ models after applying the operations inverse to standardization and logarithmization), and μ_i^{TRUE} the genuine mobility value (obtained as a result of calculations according to the Klaassen theory).

The MSE was used to assess the quality of models, in particular, when adjusting hyperparameters and as an objective function for minimization during training. To evaluate the accuracy of mobility predictions directly, the MAE and MAPE were used, as well as the median, $\mathrm{APE}_{\mathrm{MED}}$, and maximum, $\mathrm{APE}_{\mathrm{MAX}}$, values of relative error.

The general scheme of using ML models is presented in Fig. 1.

3. Results and their discussion

3.1. Symbolic regression

To describe the mobility of electrons when they are majority carriers in single-crystalline silicon, the following expressions were obtained as a result of applying SR:

$$\mu_{nn} = \frac{N_{Dn} + 1413.2}{T_n^{2.2508} + \frac{a_{nn} b_{nn}}{a_{nn} + b_{nn}}}, \tag{12a}$$

$$a_{nn} = \left(\frac{N_{Dn}}{0.873 T_n + 0.0727} \right)^{0.7212}, \tag{12b}$$

$$b_{nn} = 0.215 N_{Dn}^{0.58} + 10.5 T_n - 1.342. \tag{12c}$$

The most interesting feature is the denominator in formula (12a). The temperature dependence of the first term in it is extremely close to the dependence of the mobility associated with scattering by phonons. The form of the second term coincides with the expected expression according to the Matthiessen's rule in the presence of two scattering mechanisms. In general, expression (12) contains only nine parameters, being much simpler than that proposed in the Klaassen theory. At the same time, the error of expression (12) compared to formulas (C1)–(C10) does not exceed 1.2%; see Fig. 2, *a*. However, even such a rather small deviation is observed only at $T \approx 200$ K and $N_d \sim 10^{18}$ cm^{-3}. For the vast majority of temperature and doping level values, the APE does not exceed 0.15%.

The obtained analytical expression for the description of the mobility of minority electrons in silicon is

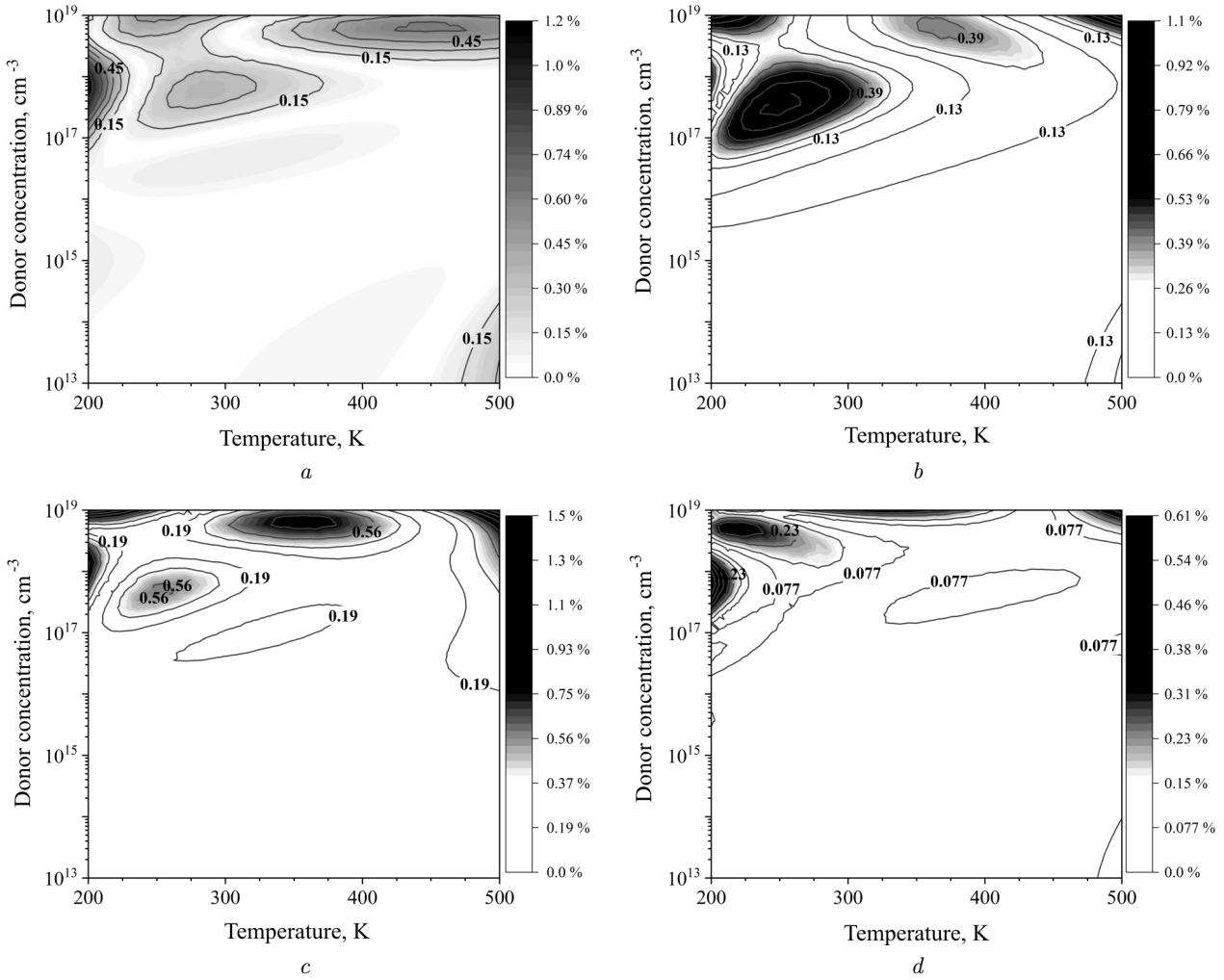

Fig. 2. Temperature and concentration dependences of the absolute relative error for the mobility of electrons (*a*, *b*) and holes (*c*, *d*) in silicon evaluated using expressions (12)–(15) in the cases where they are majority (*a*, *c*) and minority (*b*, *d*) charge carriers

given by the formulas

$$\mu_{np} = 26.3\left(\frac{N_{Dn}}{N_{Dn}+192}\right)^{0,62} + \frac{1412.3}{T_n^{2.25}+\frac{a_{np}b_{np}}{a_{np}+b_{np}}}, \quad (13a)$$

$$a_{np} = 1.92\left(\frac{N_{Dn}}{T_n+0,071}\right)^{0.717}, \quad (13b)$$

$$b_{np} = 5.7N_{Dn}^{0.103}T_n. \quad (13c)$$

The APE values, together with the results of the Klaassen model, are presented in Fig. 2, *b* as a function of temperature and acceptor concentration. In this case, the maximum discrepancies – which, however, do not exceed 1.1% – are observed at a dopant concentration of 10^{19} cm^{-3} and a temperature of about 500 K. Additional regions of increased error correspond to the intervals $T = 230$–270 K at $N_a = (3$–$6) \times 10^{17}$ cm^{-3}, as well as $T \simeq 200$ K at $N_a = 10^{19}$ cm^{-3}. In general, the evaluation error for the mobility of electrons as minority carriers is somewhat smaller than in the case where they act as majority charge carriers.

The expressions describing the hole mobility in *p*-Si,

$$\mu_{pp} = N_{Dn}^{0.448} + \frac{470}{T_n^{2.2505}+\frac{a_{pp}b_{pp}}{a_{pp}+b_{pp}}}, \quad (14a)$$

$$a_{pp} = 2.652\, N_{Dn}^{0.1669}T_n, \quad (14b)$$

$$b_{pp} = 0.578\, N_{Dn}^{0.7587}T_n^{-0.755}, \quad (14c)$$

contain the smallest number of parameters among all obtained expressions. However, the maximum errors are also the largest in this case, although they are observed in a rather narrow interval of parameters; see Fig. 2, *c*.

For minority holes, the best agreement was achieved between the values calculated using the obtained formula

$$\mu_{pn} = \frac{0.0226 \cdot N_{Dn} \cdot \ln T_n}{\ln T_n + 0.63} + \\ + \frac{113.56}{0.2414 \cdot \left[T_n^{2.94} + \left(\frac{a_{pn} \cdot b_{pn}}{a_{pn} + b_{pn}} \right)^{1.177} \right]^{0.76547}}, \tag{15a}$$

where

$$a_{pn} = 1.151 \cdot N_{Dn}^{0.6085}, \tag{15b}$$

$$b_{pn} = 4.21 \cdot T_n^{1.143}. \tag{15c}$$

and the results of the Klaassen model, which is illustrated in Fig. 2, *d*. The figure shows that in most of the investigated temperature and dopant concentration intervals, the relative error does not exceed 0.08%.

As can be seen, all obtained expressions (12)–(15) have a similar structure, being considerably simpler than formulas (C1)–(C10) in terms of the nesting depth, the total number of operators, and the number of parameters. At the same time, they provide almost identical accuracy in reproducing the results. In addition, the proposed expressions are more convenient to use not only because of their lower complexity, but also due to the possibility of using the doping impurity concentration, which is a passport characteristic of the material, as a calculation parameter instead of the concentrations of charge carriers and ionized impurities, which appear in the formulas of the Klaassen theory and require additional calculations. Of course, as is often the case, the latter advantage results in a reduction in the accuracy of the formulas obtained for silicon doped with an impurity whose ionization energy differs from 45 meV at temperatures when the impurity depletion is not yet observed. However, this restriction is not too strict, since 1) this is precisely the energy structure of the boron and phosphorus atoms, which are most commonly used to ensure impurity conductivity in silicon; 2) the depletion temperature for other possible dopants–aluminum, arsenic, gallium–is higher than 200 K (this is the lower limit for the applicability interval of the obtained formulas) only at $N_D \geq 10^{18}$ cm^{-3}; 3) the corresponding errors do not exceed 1%. In practice, the proposed formulas will be valid for any doping options.

3.2. Classical regression algorithms. Comparison of the efficiency of various approaches

Typical results of applying the optimized and trained regression models to the test dataset are shown in Fig. 3. The values of the metrics obtained when calculating the mobility by various methods are summarized in Table 1. One can see that the prediction errors grow as the mobility increases, and this trend is observed regardless of the selected algorithm, the preliminary data preparation, or the type of charge carriers. Data normalization does not actually affect the accuracy of predictions in the case of using Random Forest and Gradient Boosting, which, in general, is typical of tree-based algorithms. In the case of deep neural networks, an additional preprocessing makes sense, as it can be seen when comparing the results of the DNN_S and DNN_N networks in Table 1.

If we compare the indicators of various regression models, then the SVR_N models demonstrate results that are catastrophically poor in quality. In this case, only the median relative error remains at an acceptable level of about 15%. At the same time, the values of other metrics testify that for most of the examined temperatures and ligand concentrations, the deviations of the calculated mobility are extremely large. For other models, large errors are observed only for a few combinations of arguments ($\mathrm{APE_{MAX}}$ and MAPE or $\mathrm{APE_{MED}}$ differ significantly). The worst indicators are observed for the Gradient Boosting algorithm. The quantitative characteristics are slightly better in the case of using the Random Forest algorithm, but the differences from GB are quite insignificant. Next in the accuracy ranking are the DNN_N models (except for the maximum error, which is comparable to the indicators of the previously mentioned models) and the DNN_S ones, for which almost all indicators are approximately 1.5 times better. The best results were demonstrated by the SVR_S models.

Table 1 also quotes the metrics for the application of expressions obtained using the SR model. It can be seen that the corresponding indicators exceed only those of the SVR_S model (only by the MAPE

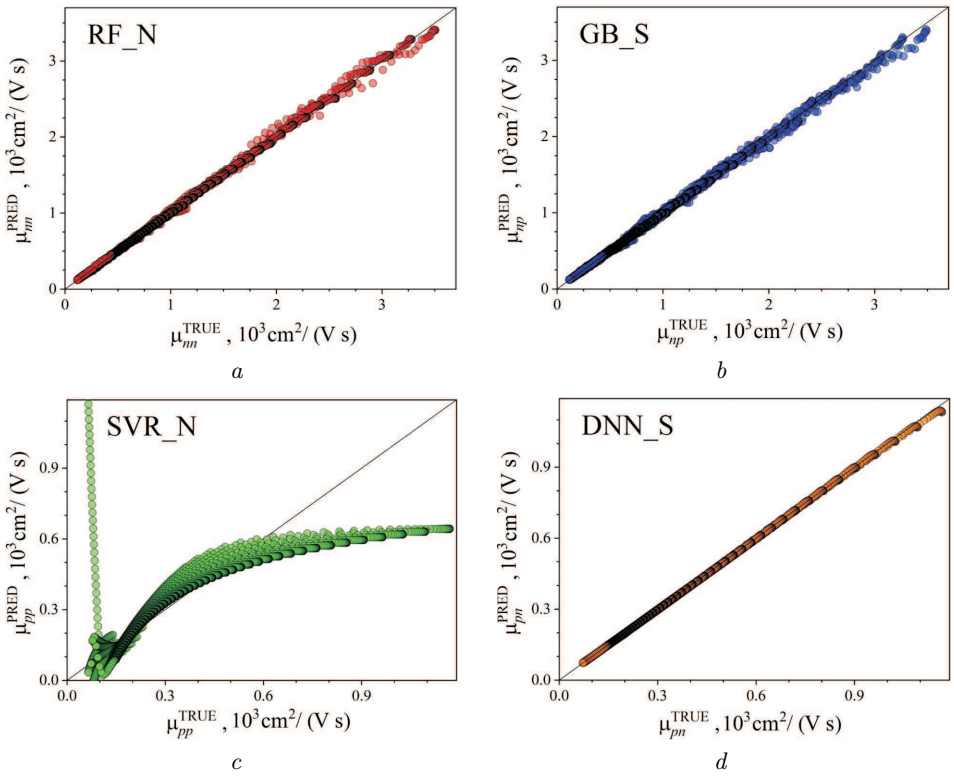

Fig. 3. Typical correspondences between the reference mobility values and the values predicted by the RF (*a*), GB (*b*), SVR (*c*), and DNN (*d*) models using the normalized (*a*, *c*) or standardized (*b*, *d*) features. The mobility of electrons (*a*, *b*) and holes (*c*, *d*) is evaluated when they are the majority (*a*, *c*) or minority (*b*, *d*) carriers. Black straight lines are identity lines, which are shown for ease of comparison

Table 1. **Metrics for evaluating the charge carrier mobility in silicon obtained using various models on the test set. The best results for each metric in predicting the mobility of different types of carriers (electrons and holes, majority and minority) are highlighted in boldface**

Model	MAPE, %				APE_{MAX}, %				APE_{MED}, %				MAE, $cm^2/(V \cdot s)$			
	μ_{nn}	μ_{np}	μ_{pp}	μ_{pn}	μ_{nn}	μ_{np}	μ_{pp}	μ_{pn}	μ_{nn}	μ_{np}	μ_{pp}	μ_{pn}	μ_{nn}	μ_{np}	μ_{pp}	μ_{pn}
RF_N	1.29	1.69	1.52	1.47	9.33	14.5	4.60	10.9	0.805	0.994	0.264	0.913	11.0	13.5	4.50	4.76
RF_S	1.42	1.77	1.46	1.41	12.3	14.4	14.5	12.6	0.852	1.04	0.744	0.872	11.6	14.1	4.40	4.76
SVR_N	46.5	51.5	32.6	33.4	1630	1750	2070	1510	14.9	17.4	13.1	12.9	220	244	68.8	73.6
SVR_S	0.108	**0.087**	**0.098**	0.082	1.71	2.16	2.26	3.56	0.088	**0.064**	**0.069**	0.050	1.20	1.03	0.394	0.410
GB_N	2.20	1.46	1.60	1.55	58.2	10.8	17.3	11.0	1.46	0.939	0.905	1.15	15.43	10.85	4.75	5.24
GB_S	1.32	1.60	1.82	1.23	1.42	11.7	15.0	8.48	0.841	1.104	1.19	0.874	11.3	13.4	5.92	4.19
DNN_N	0.925	0.942	2.01	0.529	9.39	20.0	8.07	6.02	0.621	0.702	1.893	0.383	5.23	5.37	4.22	1.39
DNN_S	0.374	0.623	0.655	0.671	2.23	3.75	5.96	2.97	0.323	0.392	0.556	0.631	3.58	3.49	2.88	1.97
SR	**0.094**	0.137	0.140	**0.050**	**1.19**	**0.992**	**1.48**	**0.596**	**0.044**	0.077	0.079	**0.026**	**0.475**	**0.708**	**0.314**	**0.115**
Arora [11]	5.35	20.3	5.62	37.8	38.2	70.7	17.6	111	3.67	16.3	5.01	32.6	45.7	103	16.0	82.6

and APE_{MED} values for silicon with hole conductivity). For the remaining 12 of 16 metrics, the best indicators are for the SR. That is, formulas (12)–(15) are superior in accuracy to regression models that use Random Forest, Gradient Boosting, and Deep Neural Networks algorithms. When compared with the Support Vector algorithm, the advantage in accuracy is not so great, but the practical use of SVR models (as well as other classical approaches to solving regression problems) requires the application of the trained models, the appropriate software, and a preliminary data preparation (the coefficients of linear

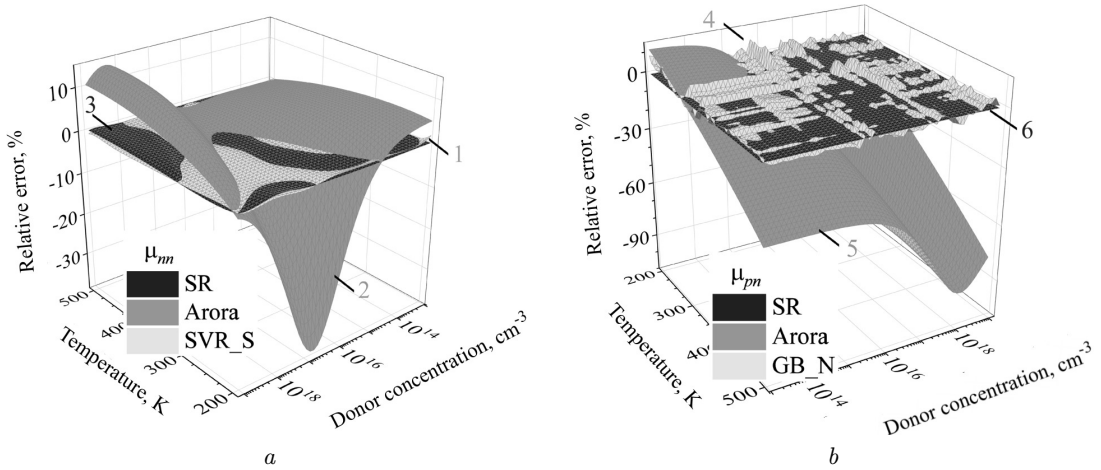

Fig. 4. Temperature and concentration dependences of the mobility calculation error for majority (*a*) and minority (*b*) carriers using various models – SVR_S (*1*), Arora (*2, 5*), SR (*3, 6*), and GB_N (*4*) – with respect to the Klaassen theory

transformations used for normalization depend on the training set). Such a process is not too complicated or critical for implementation, but it looks somewhat more difficult than calculations using the known formula. In addition, the presence of an analytical expression has a number of advantages as compared to the "black box" regression model mentioned in the Introduction.

Besides the comparison of the accuracy of mobility predictions when using various ML models, it is pertinent to confront the results of Klaassen theory with the results of other, more simplified approaches to determining μ. In this work, attention was focused on the Arora theory, as the most popular approximation among those found in the literature, and calculations were performed according to expressions (B3)–(B4). The calculated metrics and the relative errors are quoted in Table 1 and depicted in Fig. 4, respectively. For comparison, Fig. 4 also demonstrates errors for some ML models. Note that the results obtained for n-Si are similar to those obtained for silicon with hole conductivity.

By their structural complexity and the number of parameters, expressions (B3)–(B4) are quite comparable to formulas (12)–(15), but they produce much worse results, especially for minority carriers. In other words, replacing the expressions from the Klaassen theory by simpler expressions from the Arora theory leads to considerably larger errors than when using any of the ML models, except for SVR_N.

It is known that the Arora model, unlike the Klaassen approach, does not take carrier-carrier scattering into account. Therefore, for the test datasets, the value of μ was additionally calculated under the assumption that individual contributions to the total mobility are described by Arora (B3) and Dorkel (A6) relationships, and their combination was carried out according to the Matthiessen's rule. It turned out that under those conditions, the carrier-carrier scattering is extremely small: the maximum deviations of the values obtained according to the Arora-Dorkel approach from the Arora theory did not exceed 0.059% for $\mu_{n,n}$, 0.068% for $\mu_{n,p}$, 0.023% for $\mu_{p,p}$, and 0.028% for $\mu_{p,n}$. In other words, taking an additional mechanism into account did not bring the mobility values calculated in the framework of the Arora theory to more accurate values that can be obtained using the Klaassen theory and the approximations proposed in this work.

4. Conclusions

Machine learning regression models have been developed and tuned to evaluate the mobility of electrons and holes in n-Si and p-Si using the Random Forest, Gradient Boosting, Support Vector Regression, and Deep Neural Network algorithms. The prediction accuracy of the specified models was compared with that of the Klaassen theory, and the feasibility of using the Support Vector Regression and Deep Neu-

ral Network algorithms with a preliminary input data normalization was shown.

Using the Symbolic Regression algorithm, analytical expressions were derived to describe the mobility of electrons and holes in single-crystalline silicon in a temperature interval of 200–500 K and a dopant concentration interval of $10^{13} - 10^{19}$ cm^{-3}. Compared to the Klaassen model, the proposed formulas contain less than half the number of parameters, do not require a preliminary determination of the ligand ionization degree, and have a simpler structural form. At the same time, the accuracy loss is minimal: for approximately 50% of all combinations of the temperature and the doping degree, the relative error did not exceed 0.044%, 0.077%, 0.079%, and 0.026% when calculating $\mu_{n,n}$, $\mu_{n,p}$, $\mu_{p,p}$, and $\mu_{p,n}$, respectively. Compared with the Arora model, the obtained expressions are characterized by a comparable complexity, but they provide a significantly higher accuracy. This fact demonstrates the feasibility and prospects of their practical application.

APPENDIX A
Mobility dependences for a single scattering mechanism

The following expression is often used to describe the mobility $\mu_{\rm I}$ when charge carriers are scattered by ionized impurities [1, 3]:

$$\mu_{\rm I} = \frac{1.44\times10^{18}{\rm cm}^{-3}}{N_{\rm I}Z^2}\left(\frac{T}{100\,{\rm K}}\right)^{\frac{3}{2}}\times \\ \times\frac{\varepsilon^2\sqrt{m_0/m}}{\left[\lg(1+\beta_{\rm BH}^2)-\dfrac{0.434\beta_{\rm BH}^2}{1+\beta_{\rm BH}^2}\right]}, \tag{A1}$$

where $N_{\rm I}$ is the concentration of impurities with charge Ze, ε the dielectric permittivity of the semiconductor, T the temperature, m the effective carrier mass, m_0 the mass of a free electron, and the quantity $\beta_{\rm BH}$ has the form

$$\beta_{\rm BH} = \frac{T}{100\,{\rm K}}\sqrt{\frac{2.08\times10^{18}\ {\rm cm}^{-3}\,\varepsilon\, m}{16\, n_c\, m_0}}, \tag{A2}$$

and n_c is the concentration of charge carriers. This expression is called the Brooks–Herring formula. It was obtained in the framework of the relaxation time approximation for the case of an isotropic parabolic band and a weakly screened Coulomb potential. A less rigorous approximation from the physical point of view, which involves the application of the Coulomb potential with artificial truncation at small scattering angles and works better at high impurity concentrations, is called the Conwell–Weisskopf formula [1, 3],

$$\mu_{\rm I} = \frac{1.44\times10^{18}\ {\rm cm}^{-3}}{N_{\rm I}Z^2}\left(\frac{T}{100\,{\rm K}}\right)^{\frac{3}{2}}\frac{\varepsilon^2\sqrt{m_0/m}}{\lg\left(1+\beta_{\rm CW}^2\right)}, \tag{A3}$$

$$\beta_{\rm CW} = \frac{T}{100\,{\rm K}}\,\frac{\varepsilon}{16\,Z}\left(\frac{2.35\times10^{19}\ {\rm cm}^{-3}}{N_{\rm I}}\right)^{\frac{1}{3}}. \tag{A4}$$

For carrier-carrier scattering, the approach developed by Fletcher is often used [6]:

$$\mu_{cc} = \frac{\left(\frac{T}{T_{\rm ref}^{\rm F1}}\right)^{\frac{3}{2}}F_1}{\sqrt{np}\,\ln\left[1+\left(\frac{T}{T_{\rm ref}^{\rm F1}}\right)^2(np)^{-\frac{1}{3}}F_2\right]}, \tag{A5}$$

where n and p are the electron and hole concentrations, respectively; and $T_{\rm ref}^{\rm F1}$, F_1, and F_2 are constants whose values depend on the material. As was shown in Refs. [52, 53], for silicon, it is advisable to use the values $T_{\rm ref}^{\rm F1} = 300$ K, $F_1 = 1.04\times10^{21}\,({\rm cm\,V\,s})^{-1}$, and $F_2 = 7.45\times10^{12}$ cm^2; then expression (A5) is transformed into the following one (the so-called Dorkel formula):

$$\mu_{cc} = \frac{2\times10^{17}T^{\frac{3}{2}}}{\sqrt{n\,p}\,\ln\left[1+8.28\times10^8T^2\,(np)^{-\frac{1}{3}}\right]}. \tag{A6}$$

APPENDIX B
Models of carrier mobility in silicon

The Caughey–Thomas model [8] is as follows:

$$\mu^{\rm CT} = \mu_{\rm min} + \frac{\mu_{\rm max}-\mu_{\rm min}}{1+(N/N_{\rm ref})^{\alpha}}, \tag{B1}$$

where N is the ligand concentration, and the values of the constants for both types of carriers are given in Table B1.

The Masetti model [9] is given by

$$\mu_n^{\rm M} = \mu_0 + \frac{\mu_{\rm max}-\mu_0}{1+\left(\frac{n}{C_r}\right)^a} - \frac{\mu_1}{1+\left(\frac{C_s}{n}\right)^b}, \\ \mu_p^{\rm M} = \frac{\mu_0}{\exp\left(\frac{p_c}{p}\right)} + \frac{\mu_{\rm max}}{1+\left(\frac{p}{C_r}\right)^a} - \frac{\mu_1}{1+\left(\frac{C_s}{p}\right)^b}, \tag{B2}$$

where the coefficients depend on the type of doping atoms. Table B2 gives the corresponding values for boron and phosphorus.

In the Arora model [11],

$$\mu^{\rm A} = \mu_{\rm min} + \frac{\mu_0}{1+\left(\frac{N_I}{N_0}\right)^{\alpha}}, \tag{B3}$$

where $N_I = N_a^- + N_d^+$ is the total concentration of ionized ligands (N_a^- and N_d^+ are the amounts of ionized acceptors

Table B1. **Parameters for calculating the mobility according to the Caughey–Thomas model; Eq. (B1)**

Carrier type	Parameter			
	$\mu_{\rm max}$, cm^2/(V·s)	$\mu_{\rm min}$, cm^2/(V·s)	α	$N_{\rm ref}$, cm^{-3}
Electrons	1330	65	0.72	8.5×10^{16}
Holes	495	47.7	0.76	6.3×10^{16}

Table B2. **Parameters for calculating the mobility according to the Masetti model; Eq. (B2)**

Parameter	Dopant	
	Phosphorus	Boron
μ_0, $\mathrm{cm}^2/(\mathrm{V}\cdot\mathrm{s})$	68.5	44.9
$\mu_{\max}$, $\mathrm{cm}^2/(\mathrm{V}\cdot\mathrm{s})$	1414	470.5
μ_0, $\mathrm{cm}^2/(\mathrm{V}\cdot\mathrm{s})$	56.1	29.0
C_r, cm^{-3}	9.2×10^{16}	2.23×10^{17}
C_s, cm^{-3}	3.41×10^{20}	6.10×10^{20}
a	0.711	0.719
b	1.98	2.00
p_c, cm^{-3}	–	9.23×10^{16}

Table B3. **Parameters for calculating the mobility according to the Arora model; Eqs. (B3)–(B4)**

Parameter	Carrier type			
	Electrons		Holes	
	Majority [11]	Minority [13]	Majority [11]	Minority [14]
T_{ref}, K	300	295	300	292
$\mu_{\min}^{\mathrm{ref}}$, $\mathrm{cm}^2/(\mathrm{V}\cdot\mathrm{s})$	88	232	54,3	130
μ_0^{ref}, $\mathrm{cm}^2/(\mathrm{V}\cdot\mathrm{s})$	1252	1180	407	370
N_0^{ref}, $1/\mathrm{cm}^3$	1.26×10^{17}	8×10^{16}	2.35×10^{17}	8×10^{17}
α^{ref}	0.88	0.9	0.88	1.25
β_1	–0.57			
β_2	–2.33		–2.23	
β_3	2.4			
β_4	–0.146			

and donors per unit volume, respectively), and the remaining coefficients have a similar temperature dependence:

$$\mu_{\min}=\mu_{\min}^{\mathrm{ref}}\left(\frac{T}{T_{\mathrm{ref}}}\right)^{\beta_1},\quad \mu_0=\mu_0^{\mathrm{ref}}\left(\frac{T}{T_{\mathrm{ref}}}\right)^{\beta_2},$$
$$N_0=N_0^{\mathrm{ref}}\left(\frac{T}{T_{\mathrm{ref}}}\right)^{\beta_3},\quad \alpha=\alpha^{\mathrm{ref}}\left(\frac{T}{T_{\mathrm{ref}}}\right)^{\beta_4}. \tag{B4}$$

(see Table B3). The constants are given in Table B2.

APPENDIX C
Evaluation of mobility according to the Klaassen (Philips) model

In this case [12], similar formulas with different numerical coefficients are used to calculate the mobility of both electrons and holes, regardless of whether they are majority or minority carriers. Namely,

Table C1. **Parameters for calculating the mobility according to the Klaassen model by Eqs. (C2)–(C3)**

Carrier type	Parameter			
	$\mu_{\max}$, $\mathrm{cm}^2/(\mathrm{V}\cdot\mathrm{s})$	$\mu_{\min}$, $\mathrm{cm}^2/(\mathrm{V}\cdot\mathrm{s})$	α	N_{ref}, cm^{-3}
Electrons	1414	68.5	0.711	9.2×10^{16}
Holes	495	44.9	0.719	2.23×10^{17}

Table C2. **Parameters for calculating the mobility according to the Klaassen model using Eqs. (C6) and (C7)**

S_1	S_2	S_3	S_4	S_5	S_6	S_7
0.89233	0.41372	0.19778	0.28227	0.005978	1.80618	0.72169
r_1	r_2	r_3	r_4	r_5	r_6	
0.7643	2.2999	6.5502	2.3670	–0.01552	0.6478	

$$\mu^{\mathrm{K}}=\frac{\mu_{\mathtt{L}}\,\mu_{\mathtt{DA}}}{\mu_{\mathtt{L}}+\mu_{\mathtt{DA}}}, \tag{C1}$$

where

$$\mu_{\mathtt{L}}=\mu_{\max}\left(\frac{300}{T}\right)^{2,25}, \tag{C2}$$

$$\mu_{\mathtt{DA}}=\frac{\mu_{\max}^2}{\mu_{\max}-\mu_{\min}}\,\frac{N_{\mathrm{sc}}}{N_{\mathrm{eff}}}\left(\frac{N_{\mathrm{ref}}}{N_{\mathrm{sc}}}\right)^{\alpha}\left(\frac{T}{300}\right)^{3\alpha-\frac{3}{2}}+$$
$$+\frac{\mu_{\max}\,\mu_{\min}}{\mu_{\max}-\mu_{\min}}\,\frac{n+p}{N_{\mathrm{eff}}}\left(\frac{300}{T}\right)^{\frac{1}{2}}, \tag{C3}$$

and the constants are given in Table C1.

The quantities N_{sc} and N_{eff} depend on the temperature and the concentrations of carriers and ionized ligands; their analytical formulas depend on the carrier type. Namely, when determining the mobility of electrons,

$$N_{\mathrm{sc}}=N_d^+ + N_a^- + p, \tag{C4a}$$
$$N_{\mathrm{eff}}=N_d^+ + N_a^-\cdot G_n(P_n,T)+\frac{p}{F_n(P_n,T)}, \tag{C5a}$$

whereas for the mobility of holes,

$$N_{\mathrm{sc}}=N_a^- + N_d^+ + n, \tag{C4b}$$
$$N_{\mathrm{eff}}=N_a^- + N_d^+\cdot G_p(P_p,T)+\frac{n}{F_p(P_p,T)}. \tag{C5b}$$

In turn, the functions $G_{n(p)}$, $F_{n(p)}$, and $P_{n(p)}$ have the form

$$G_n=1-S_1\left[S_2+\left(\frac{m_0}{m_e}\frac{T}{300}\right)^{S_4}P_n\right]^{-S_3}+$$
$$+S_5\left[\left(\frac{m_e}{m_0}\frac{300}{T}\right)^{S_7}P_n\right]^{-S_6}, \tag{C6a}$$

$$G_p = 1 - S_1 \left[S_2 + \left(\frac{m_0}{m_h} \frac{T}{300} \right)^{S_4} P_p \right]^{-S_3} + \\ + S_5 \left[\left(\frac{m_h}{m_0} \frac{300}{T} \right)^{S_7} P_p \right]^{-S_6}, \quad \text{(C6b)}$$

$$F_n = \frac{r_1 P_n^{r_6} + r_2 + r_3 \dfrac{m_e}{m_h}}{P_n^{r_6} + r_4 + r_5 \dfrac{m_e}{m_h}}, \quad F_p = \frac{r_1 P_p^{r_6} + r_2 + r_3 \dfrac{m_h}{m_e}}{P_n^{r_6} + r_4 + r_5 \dfrac{m_h}{m_e}}, \quad \text{(C7)}$$

$$P_n = (P_{bn} + P_{cn})^{-1}, \quad P_p = \left(P_{bp} + P_{cp}\right)^{-1}, \quad \text{(C8)}$$

$$P_{bn} = \frac{3.83 \left(\frac{m_0}{m_e}\right)}{\frac{1.36\times10^{26}}{N_d^+ + p} \left(\frac{T}{300}\right)^2}, \quad P_{bp} = \frac{3.83 \left(\frac{m_0}{m_h}\right)}{\frac{1.36\times10^{26}}{N_a^- + n} \left(\frac{T}{300}\right)^2}, \quad \text{(C9)}$$

where m_e and m_h are the effective masses of the electron and hole, respectively; and the values of the constants in expressions (C6) and (C7) are given in Table C2. In the case of minority carriers, $P_{cn} = 0$, $P_{cp} = 0$; for the majority ones,

$$P_{cn} = \frac{\left(Z_n \sqrt[3]{N_d^+}\right)^2}{1.79 \cdot 10^{14}\, T^2}, \quad P_{cp} = \frac{\left(Z_p \sqrt[3]{N_a^-}\right)^2}{1.79\, 10^{14}\, T^2}, \quad \text{(C10a)}$$

$$Z_n = \frac{1.21 + \frac{1.6\times10^{41}}{\left(N_d^+\right)^2}}{0.21 + \frac{1.6\times10^{41}}{\left(N_d^+\right)^2}}, \quad Z_p = \frac{1.5 + \left(\frac{7.2\, 10^{20}}{N_a^-}\right)^2}{0.5 + \left(\frac{7.2\, 10^{20}}{N_a^-}\right)^2}. \quad \text{(C10b)}$$

1. C. Hamaguchi. *Basic Semiconductor Physics*. 4th edition (Springer Cham, 2023) [ISBN: 978-3-031-25510-6].
2. J. Leveillee, X. Zhang, E. Kioupakis, F. Giustino. Ab initio calculation of carrier mobility in semiconductors including ionized-impurity scattering. *Phys. Rev. B* **107**, 125207 (2023)
3. K. Seeger. *Semiconductor Physics. An Introduction*. 9th edition (Springer Berlin, 2004) [ISBN: 978-3-540-21957-6].
4. K.W. Böer, U.W. Pohl. *Semiconductor Physics* 2nd edition (Springer Cham, 2023) [ISBN: 978-3-031-18285-3].
5. E. Bourbaba, S. Kadri, M. Bensafi, S. Larguech, Y. Menni, B.M. Alshammari, L. Kolsi. Empirical model integration for accurate charge carrier mobility simulation in silicon mosfets. *Open Physics* **23**, 20250248 (2025).
6. N.H. Fletcher. The high current limit for semiconductor junction devices. *Proc. IRE* **45**, 862 (1957).
7. S. Rudra, D. Rao, S. Poncé, B. Saha. Dominant scattering mechanisms in limiting the electron mobility of scandium nitride. *Nano Lett.* **24**, 11529 (2024).
8. D. Caughey, R. Thomas. Carrier mobilities in silicon empirically related to doping and field. *Proc. IEEE* **55**, 2192 (1967).
9. G. Masetti, M. Severi, S. Solmi. Modeling of carrier mobility against carrier concentration in arsenic-, phosphorus-, and boron-doped silicon. *IEEE Trans. Electron Devices* **30**, 764 (1983).
10. S. Berrada, H. Carrillo-Nunez, J. Lee, C. Medina-Bailon, T. Dutta, O. Badami, F. Adamu-Lema, V. Thirunavukkarasu, V. Georgiev, A. Asenov. Nano-electronic simulation software (ness): A flexible nano-device simulation platform. *J. Comput. Electron.* **19**, 1031 (2020).
11. N. Arora, J. Hauser, D. Roulston. Electron and hole mobilities in silicon as a function of concentration and temperature. *IEEE Trans. Electron Devices* **29**, 292 (1982).
12. D. Klaassen. A unified mobility model for device simulation – I. Model equations and concentration dependence. *Solid-State Electron.* **35**, 953 (1992).
13. S. Swirhun, Y.-H. Kwark, R. Swanson. Measurement of electron lifetime, electron mobility and band-gap narrowing in heavily doped p-type silicon. In: *Proc of the 1986 International Electron Devices Meeting, Los Angeles, CA, USA, December 07–10, 1986*, p. 24.
14. J. del Alamo, S. Swirhun, R. Swanson. Simultaneous measurement of hole lifetime, hole mobility and bandgap narrowing in heavily doped *n*-type silicon. In: *Proc of the 1985 International Electron Devices Meeting, Washington, DC, USA, December 01-04, 1985*, p. 290.
15. D.L. Rode, J.S. Cetnar. Electron mobility of heavily doped semiconductors including multiple scattering by ionized impurities. *J. Appl. Phys.* **134**, 075701 (2023).
16. T. Sadi, C. Medina-Bailon, M. Nedjalkov, J. Lee, O. Badami, S. Berrada, H. Carrillo-Nunez, V. Georgiev, S. Selberherr, A. Asenov. Simulation of the impact of ionized impurity scattering on the total mobility in si nanowire transistors. *Materials* **12**, 124 (2019).
17. Z. Wang, Z. Tang, A. Guo, X. Luo, C. Cao, Y. Yuan, X. Zhang, L. Liu, J. Li, Y. Cao, O. Shao, S. Hu, S. Chen, Y. Zhao, X. Kou. Temperature-driven gate geometry effects in nanoscale cryogenic mosfets. *IEEE Electron Device Lett.* **41**, 661 (2020).
18. L. Abenante. Incomplete activation and ionization of dopants in si at room temperature. *AIP Adv.* **13**, 015109 (2023).
19. D.J. Cummings, A.F. Witulski, H. Park, R.D. Schrimpf, S.E. Scott, M.E. Low. Mobility modeling considerations for radiation effects simulations in silicon. *IEEE Trans. Nucl. Sci.* **57**, 2318 (2010).
20. Q. Wu, A. Sojka, B.D. Price, N.I. Agladze, A. Yadav, S.L. Pain, J.D. Murphy, T. Niewelt, M.S. Sherwin. Two-fluid mobility model from coupled hydrodynamic equations for simulating laser-driven semiconductor switches. *Phys. Rev. Appl.* **24**, 014007 (2025).
21. S. Noor Mohammad, A.V. Bemis, R.L. Carter, R.B. Renbeck. Temperature, electric field, and doping dependent mobilities of electrons and holes in semiconductors. *Solid-State Electron.* **36**, 1677 (1993).
22. Y.-N. Wu, X.-G. Zhang, S. T. Pantelides. First-principles calculations reveal controlling principles for carrier mobilities in semiconductors. *Semicond. Sci. Technol.* **31**, 115016 (2016).
23. D.-Y. Liu, L.-M. Xu, X.-M. Lin, X. Wei, W.-J. Yu, Y. Wang, Z.-M. Wei. Machine learning for semiconductors. *Chip* **1**, 100033 (2022).

24. R. Li, E. Lee, T. Luo. A unified deep neural network potential capable of predicting thermal conductivity of silicon in different phases. *Mater. Today Phys.* **12**, 100181 (2020).
25. R. Li, E. Lee, T. Luo. Physics-informed deep learning for solving coupled electron and phonon boltzmann transport equations. *Phys. Rev. Appl.* **19**, 064049 (2023).
26. R. Li, J. Zhou, J.-X. Wang, T. Luo. Physics-informed bayesian neural networks for solving phonon boltzmann transport equation in forward and inverse problems with sparse and noisy data. *ASME J. Heat and Mass Transfer* **147**, 032501 (2024).
27. C. Fai, A.J. Ladd, C.J. Hages. Machine learning for enhanced semiconductor characterization from time-resolved photoluminescence. *Joule* **6**, 2585 (2022).
28. Y. Xu, A. V. Lalwani, K. Arora, Z. Zheng, A. Renteria, D.G. Senesky, P. Wang. Hall-effect sensor design with physics-informed gaussian process modeling. *IEEE Sensors J.* **22**, 22519 (2022).
29. X. Chen, S. Lu, Q. Chen, Q. Zhou, J. Wang. From bulk effective mass to 2d carrier mobility accurate prediction via adversarial transfer learning. *Nat. Commun.* **15**, 5391 (2024).
30. J.H. Hong, C.H. Lee, H.W. Kim, D.W. Jeon, J.H. Jun, Y.-S. Kim, J.-S. Bae, S. Heo, S. Lee, J. Na, J. You, S. Hong, H. Cho, J.-S. Park, S.B. Cho. Ai-driven quantitative review of mobility–stability trade-off in oxide semiconductors. *Nano Convergence* **13**, 4 (2026).
31. T. Nematiaram, Z. Lamprou, Y. Moshfeghi. Accelerating the discovery of high-mobility molecular semiconductors: a machine learning approach. *Chem. Commun.* **61**, 3676 (2025).
32. P. Reiser, M. Konrad, A. Fediai, S. Léon, W. Wenzel, P. Friederich. Analyzing dynamical disorder for charge transport in organic semiconductors via machine learning. *J. Chem. Theory Comput.* **17**, 3750 (2021).
33. A.K. Pimachev, S. Neogi. First-principles prediction of electronic transport in fabricated semiconductor heterostructures via physics-aware machine learning. *npj Comput. Mater.* **7**, 93 (2021).
34. V. Bhat, B. Ganapathysubramanian, C. Risko. Rapid estimation of the intermolecular electronic couplings and charge-carrier mobilities of crystalline molecular organic semiconductors through a machine learning pipeline. *J. Phys. Chem. Lett.* **15**, 7206 (2024).
35. T. Tan, D. Wang. Machine learning based charge mobility prediction for organic semiconductors. *J. Chem. Phys.* **158**, 094102 (2023).
36. K.M. Mamun, N. Pala, M.S.A. Shawkat. A comprehensive review of machine learning approaches for semiconductor device modeling and simulation. *IEEE Access* **13**, 162969 (2025).
37. P. Raut, D.K. Panda, A.K. Goyal. A comprehensive review on next-generation modeling and optimization for semiconductor devices. *IEEE Access* **13**, 123724 (2025).
38. R. Khatua, B. Das, A. Mondal. Physics-informed machine learning with data-driven equations for predicting organic solar cell performance. *ACS Appl. Mater. Interfaces* **16**, 57467 (2024).
39. R. Couderc, M. Amara, M. Lemiti. Reassessment of the intrinsic carrier density temperature dependence in crystalline silicon. *J. Appl. Phys.* **115**, 093705 (2014).
40. R. Pässler. Dispersion-related description of temperature dependencies of band gaps in semiconductors. *Phys. Rev. B* **66**, 085201 (2002).
41. A. AlQurashi, C. Selvakumar. A new approximation of Fermi-Dirac integrals of order 1/2 for degenerate semiconductor devices. *Superlattices Microstruct.* **118**, 308 (2018).
42. A. Tonda. Review of pysr: high-performance symbolic regression in python and julia. *Genet. Program. Evol. M.* **26**, 7 (2024).
43. D. Angelis, F. Sofos, T. E. Karakasidis. Artificial intelligence in physical sciences: Symbolic regression trends and perspectives. *Arch. Comput. Methods Eng.* **30**, 3845 (2023).
44. V. Hruska, A. Furmanova, M. Bednarik. Analytical formulae for design of one-dimensional sonic crystals with smooth geometry based on symbolic regression. *J. Sound Vibration* **597**, 118821 (2025).
45. B.L. Davis, Z. Jin. Discovery of a planar black hole mass scaling relation for spiral galaxies. *Astrophys. J. Lett.* **956**, L22 (2023).
46. V.V. Kuryliuk, O.Y. Olikh. Thermal conductivity of nanoporous silicon: Molecular dynamics simulations and machine learning prediction. *Low Temp. Phys.* **52**, 50 (2026).
47. T. Mengel, P. Steffanic, C. Hughes, A.C.O. da Silva, C. Nattrass. Interpretable machine learning methods applied to jet background subtraction in heavy-ion collisions. *Phys. Rev. C* **108**, L021901 (2023).
48. Y. Li, H. Wang, Y. Li, H. Ye, Y. Zhang, R. Yin, H. Jia, B. Hou, C. Wang, H. Ding, X. Bai, A. Lu. Electron transfer rules of minerals under pressure informed by machine learning. *Nat. Commun.* **14**, 1815 (2023).
49. M. Cranmer. Interpretable machine learning for science with pysr and symbolicregression.jl. arXiv:2305.01582v3 [astro-ph.IM]
50. M.F. Hanif, M.U. Siddique, J. Si, M.S. Naveed, X. Liu, J. Mi. Enhancing solar forecasting accuracy with sequential deep artificial neural network and hybrid random forest and gradient boosting models across varied terrains. *Advanced Theory and Simulations* **7**, 2301289 (2024.
51. T. Akiba, S. Sano, T. Yanase, T. Ohta, M. Koyama. Optuna: A next-generation hyperparameter optimization framework. In: *Proc of the 25th ACM SIGKDD Int. Conf. Knowl. Discov. Data Mining, Anchorage, AK, USA, August 04-08, 2019*, p. 2623.
52. S.C. Choo. Theory of a forward-biased diffused-junction p-l-n rectifier-part i: Exact numerical solutions. *IEEE Trans. Electron Devices* **19**, 954 (1972).

53. J. Dorkel, P. Leturcq. Carrier mobilities in silicon semi-empirically related to temperature, doping and injection level. *Solid-State Electron.* **24**, 821 (1981).

Received 05.03.26.
Translated from Ukrainian by O.I. Voitenko

О.Я. Оліх

ЗАСТОСУВАННЯ МОДЕЛЕЙ МАШИННОГО НАВЧАННЯ ДЛЯ ЕФЕКТИВНОЇ ОЦІНКИ РУХЛИВОСТІ НОСІЇВ У КРЕМНІЇ

У роботі досліджено застосування моделей машинного навчання (RF, GB, SVR, DNN) і символьної регресії (SR) для оцінки рухливості носіїв у монокристалічному кремнії (T = 200–500 K, $N_D = 10^{13}$–10^{19} см$^{-3}$). Отримані за допомогою SR компактні аналітичні вирази мають удвічі менше параметрів порівняно з моделлю Клаассена і не потребують попереднього розрахунку іонізації домішок, забезпечуючи водночас відносну похибку меншу за 0,1% для більшості випадків. Порівняльний аналіз показав, що моделі SR і SVR суттєво кращі за наближення Арора за точністю, особливо для неосновних носіїв. Запропонований підхід є перспективним для TCAD-систем, оскільки дає змогу значно зменшити обчислювальні витрати при збереженні високої достовірності моделювання.

Ключові слова: рухливість носіїв, кремній, модель Клаассена, символьна регресія, машинне навчання.